Journal of Environmental Chemical Engineering 11 (2023) 111466

Contents lists available at ScienceDirect

Journal of Environmental Chemical Engineering

journal homepage: www.elsevier.com/locate/jece

Role of the different catalytic sites in the H_2O_2-mediated aqueous-phase furfural partial oxidation

Paula Rapado, Laura Faba, Salvador Ordóñez *

Catalysis, Reactors and Control Research Group (CRC), Dept. of Chemical and Environmental Engineering, University of Oviedo, Julián Clavería s/n, 33006 Oviedo, Spain

ARTICLE INFO

Editor: Javier Marugan

Keywords:
Furfural upgrading
Aqueous-phase oxidation
Heterogeneous catalysis
Bifunctional catalysts
Au
TiO2

ABSTRACT

The potential of hydrogen peroxide as oxidizing agent for furfural partial oxidation is studied in this work. Hydrogen peroxide is proposed as an alternative to air, the most typical oxidant, to reduce the severity and complexity of the process, as the reaction occurs in the liquid phase at ambient pressure. Comparing the activity of different catalysts and the selectivity for different oxidation products, including furoic acid, 2(5 H)furanone, and maleic and malic acids, a comprehensive mechanistic kinetic model is presented. This model identifies the critical catalytic properties ruling the selectivity of the process for each target compound. The results of this study emphasize the role of acidity in promoting the oxidations, the function of basicity for stabilizing the intermediate acids, and the impact of redox properties and metal particle size, which synergistically influence selectivity. This study concludes that Au/TiO_2 is the optimum catalyst to produce furoic acid (42% of selectivity). Additionally, Pt/MgZr selectively produces 2(5 H)furanone (100%), and Pd/TiO_2 and Pt/CeO_2 maximize the production of maleic acid (76.5%) and malic acid (78.5%), respectively.

1. Introduction

Lignocellulosic-based biorefineries represent the most promising and feasible alternatives to petroleum refineries to produce essential bulk chemicals needed in the current chemical processes. The extensive number of compounds required, involving polymers, liquid fuels, lubricants, agrochemicals, and pharmaceuticals, among others, can be obtained by specific chemical routes based on a limited number of key compounds, known as bioplatform molecules [1,2].

Furfural stands out as one of the most interesting bioplatform molecules. This five-carbon cyclic aldehyde is derived through the acid-catalyzed dehydration of pentoses obtained from the hemicellulose fraction of biomass [3–5]. Given the low value of this fraction, pathways centered around furfural offers an added advantage from both a circular economy and sustainability perspective. At this point, furfural catalytic oxidation is described as one of the interesting alternatives to produce various commodities, using air, molecular O_2, or hydrogen peroxide (H_2O_2) as oxidizing agents [6,7].

When using molecular oxygen for this oxidation, furoic acid (FCA) can be obtained with high selectivity [8]. FCA is the chemical precursor of 2,5-furandicarboxylic acid (FDCA), a crucial sustainable monomer with promising applications in the synthesis of green polymers. FDCA has the potential to replace terephthalic acid, one of the most widely used petroleum-based monomers, in the manufacture of polyethylene terephthalate (PET) [9]. Previous studies demonstrate a high activity in an O_2-rich atmosphere with typical oxidizing metals [10], achieving FCA yields of 63% and 69% with $Au/Mg(OH)_2$ and $Pd/Mg(OH)_2$ [11]. These yields increase up to 92% when using Ag_2O/CuO [12] or MnO_2 @CeO_2 [13].

However, this process requires temperatures above 120 ºC and high pressures, increasing the operation costs and promoting furfural polymerization. Some of these studies work with very high catalytic loadings (up to 20%w/w), which limits the applicability in a future scale-up of this approach, and strong basic conditions (NaOH) are still needed to prevent catalytic deactivation due to leaching or the permanent adsorption of furoic acid on the metal nanoparticles [14,15].

Using H_2O_2 as an alternative oxidizing agent, which is considered a green oxidant that does not produce any waste, prevents these drawbacks since the reaction occurs at softer temperatures (both reactants are in the liquid phase). The natural H_2O_2 decomposition leads to an autocatalytic process, further enhanced by the acids produced in the reaction mixture (homogeneous catalysis) [16]. These advantages, as well as the

* Corresponding author.
E-mail address: sordonez@uniovi.es (S. Ordóñez).

https://doi.org/10.1016/j.jece.2023.111466
Received 5 September 2023; Received in revised form 22 October 2023; Accepted 9 November 2023
Available online 11 November 2023

significant growth in industrial H_2O_2 production in recent decades and the possibility of in situ generation via photocatalytic or electrocatalytic methods justify the increasing interest in researching new and greener production processes (including direct synthesis) and new applications of this green industrial oxidant [17].

The furfural oxidation using H_2O_2 has been studied in the literature describing an intricate mechanistic pathway marked by a combination of parallel and sequential reaction steps. Previous literature has primarily focused on the synthesis of diacids or acid anhydrides, particularly maleic [18–26] and succinic acid [27–29], and, at lower extent, 2-(5 H)furanone (FN) [30–32] and furoic acid [33]. In most cases, relatively low selectivities are reported, due to the high reactivity of H_2O_2 and the coexistence of different reaction pathways.

Despite these individual studies, there is gap in systematic research aimed at proposing a comprehensive mechanism and determining the catalytic properties that optimize the yields of each interesting compound: FCA, MA, MAL, and FN. To our knowledge, only a previous work proposed a simplified mechanism based on homogeneous catalysis [32], without considering the presence of solid catalysts. A more complete mechanistic analysis was done by Murzin and co-workers [6], at different temperatures, but without distinguishing between homogeneous and heterogeneous contributions, and not considering the impact on the H_2O_2 decomposition rate. Regarding the catalytic properties that influence selectivity, it is established that the introduction of acid/basic or redox activity can either inhibit or promote different steps [16,34]. Consequently, basic materials promote the production of FCA, whereas acidic materials enhance a parallel route, yielding 2-hydroxyfuran (HF) as the first intermediate [35].

In this study, we assess several materials as potential catalysts for the partial oxidation of furfural using H_2O_2. Four bulk oxides with different catalytic properties were used in this work: TiO_2 and CeO_2, representing redox materials, and MgAl and MgZr, as typical mixed oxides with basic-acid sites. To enhance the catalytic activity, bifunctional materials were prepared by incorporating Au, Pd, and Pt, three of the most active metals for oxidations [36,37]. These four chosen supports have been previously proposed in different studies using lignocellulosic platform molecules. Thus, CeO_2 has been successfully tested in the selective oxidation of HMF, highlighting the close contact between metal and support obtained, and the crucial role of ceria defects in the oxidation [38,39]. TiO_2 has been widely used as support for bifunctional catalysts used in HMF oxidations, revealing a strong interaction with metal nanoparticles that alters the parent properties, increasing the surface area and the concentration of active sites, which contributes to high activity, selectivity, and stability [40,41]. Hydrotalcite-derived mixed oxides (MgAl) and other oxides (including Mg and Zr) were also considered for the HMF oxidation [42,43], mainly using Rh as the metal active site. Despite the limited literature on these materials in oxidations, they are widely used in other reactions involving furfural, such as condensation [44] or hydrogenation [45]. Thus, a good activity in this reaction could expand their versatility, increasing the spectrum of reactions related to biomass-derived molecules that can catalyze.

The reactions have been studied in a stirred batch reactor, and the results were fitted to a kinetic model that accounts for both homogeneous and heterogeneous contributions. This modeling not only aids in understanding the reaction pathways and the role of the different catalyst sites but also facilitates the optimization of the reactor design for renewable production of different commodities.

2. Experimental section

2.1. Catalysts preparation

TiO_2 (P25, Sigma Aldrich) was calcined in air for 2 h (5 ºC·min^{-1}) at 500 ºC to activate it [46]. CeO_2, MgAl and MgZr were synthetized in laboratory, as detailed in the Supplementary Information.

Metal modified catalysts: Pd and Pt, (1 wt% as theoretical metal loading) were supported using the incipient wetness impregnation method and $Pd(NH_3)_4(NO_3)_2$ and $Pt(NH_3)_4(NO_3)_2$ as precursors (Sigma Aldrich, >99.99%). The Au was deposited at 1% wt. into the different supports by deposition-precipitation method [46] using $HAuCl_4{\cdot}3\ H_2O$ (Sigma Aldrich, 99%) as precursor. All the materials were calcined for 3 h at the same temperature as their bulk materials (i.e., 400, 500, 600, and 700 ºC for CeO_2, TiO_2, MgZr, and MgAl) [16,47]. The materials were reduced in H_2 (10 v/v% in Ar) for 4 h, at 300 ºC for those catalysts with Au, and 400 ºC for the rest of them (in all the cases, with a slope of 5 ºC·min^{-1}) [48–50].

2.2. Catalysts characterization

Morphological properties (surface area, pore diameter and pore volume) were determined by N_2 physisorption at − 196 ºC using an ASAP 2020 (Micromeritics), applying the BET and BJH approaches (desorption data used for the pore diameter and volume). The same instrument was used to determine the particle size and metal dispersion by carbon monoxide chemisorption at 35 ºC.

These data were corroborated by transmission electronic microscopy (TEM), using a JEOL JEL 2100 microscope. Histograms and average particle size were calculated by analyzing at least 100 particles in each sample, using the software Confocal ImageJ. The metal dispersion was calculated according to Eq. (1), where $v_m, a_m, and < d_p >$ correspond to volume, surface, and average particle diameter, respectively:

$$D(\%) = \frac{6 \cdot \frac{v_m}{a_m}}{< d_p >} \cdot 100 \qquad \text{Eq. (1)}$$

The crystallographic structure of the mixed oxides was determined by X-ray diffraction (XRD) using a Philips PW 1710 diffractometer, working with a CuK_α line (1.54 Å) in the 2θ range between 5° and 80°, at a scanning rate of 2° min^{-1}.

The metal loading of the bifunctional catalysts was determined by Inductively Coupled Plasma Mass Spectrometer (ICP-MS) using a HP 7900 of Agilent. Approximately 50 mg of the sample were inserted into a microwave-assisted Teflon bomb; adding HCl (2.25 mL) and HNO_3 (0.75 mL) to dissolve the sample.

The surface chemistry was analysed by temperature programmed desorption (TPD) in a Micromeritics 2900 TPD/TPR. 50 mg of solid were pretreated in He flow and saturated with CO_2 or NH_3 to determine the basicity or acidity, respectively. The evolution of CO_2 and NH_3 signals were followed using a Pfeiffer Vacuum Omnistar Prisma mass spectrometer while the temperature increases at 2.5 C·min^{-1} from 25 to 550 ºC. Signals were quantitatively related to concentration values after the corresponding calibration.

2.3. Reaction studies

Reactions were carried out in a 0.5 L stirred batch autoclave reactor (Autoclave Engineers EZE seal) equipped with a backpressure regulator and a PID temperature controller. The system was loaded with the catalyst (0.5 g, 50–80 μm) and 215 mL of an aqueous solution of furfural (0.6 M). Once the desired temperature was reached (50 ºC), 35 mL of a H_2O_2 (33%, Sigma Aldrich) solution were added to achieve 1.5 M of H_2O_2 and 0.5 M of FFL in a total volume of 250 mL. Air was purged with N_2, and the oxidation was carried out with 10 bar of N_2 with a stirring of 700 rpm for 8 h. Samples were taken from the sampling port, filtered using a 0.22 μm nylon syringe filter, and diluted in a 1:2 ratio to avoid signal saturations during the analysis.

The evolution of the different involved compounds (organics and H_2O_2) was quantified by HPLC (1200 Series, Agilent) equipped with a RI detector and a Hi-Plex H column, using 0.5 mL·min^{-1} of 0.5 mM H_2SO_4 solution as mobile phase and commercial standards for the identification and calibration. Each sample was analysed at least twice, with an error margin of less than 5%. The analysis of the reaction is present in terms of

conversion, selectivity, yield, and carbon balance closure, according to the following expressions:

$$x_{FFL} \quad (\%) = \frac{C_{FFL,0} - C_{FFL,t}}{C_{FFL,0}} \cdot 100 \tag{2}$$

$$x_{H_2O_2} \quad (\%) = \frac{C_{H_2O_2,0} - C_{H_2O_2,t}}{C_{H_2O_2,0}} \cdot 100 \tag{3}$$

$$Selectivity \quad (\%) = \frac{n_i \cdot C_i}{\sum(n_i \cdot C_i)} \cdot 100 \tag{4}$$

$$Yield \quad (\%) == \frac{n_i \cdot C_i}{5 \cdot C_{FFL,0}} \cdot 100 \tag{5}$$

$$C.B.(\%) = \frac{\sum(n_i \cdot C_i)}{5 \cdot C_{FFL}} \cdot 100 \tag{6}$$

MATLAB code was used to perform the kinetic calculations and to solve the set of ordinary differential equations ("ode45″) that mathematically explains the mechanism proposed. All the experimental data were considered for these calculations to ensure that data provided represent the behavior of all the catalysts tested. The fitting of the unknown parameters was accomplished by the least-square method using the "lsqcurvefit" function and the Levenberg-Marquardt algorithm.

3. Results and discussion

3.1. Reaction pathway in absence of heterogeneous catalysts

According to literature [32], compounds with five but also four carbon atoms are expected to be obtained during the furfural oxidation, releasing formic acid that acts as a homogeneous catalyst. Considering the high oxidation capacity of H_2O_2, a contribution of the autocatalytic process is not discarded, with the subsequent formic acid production that triggers the homogeneous catalytic mechanism. Thus, a correct study of the heterogeneous catalytic mechanism requires a preliminary analysis of these concomitant effects.

An initial experiment in the absence of heterogeneous catalysts was carried out at 50 ºC, with a 3/1 H_2O_2/furfural molar ratio, to study the influence of autocatalytic and homogeneous catalytic mechanisms. The evolution of reactants and products concentration is plotted in Fig. 1. A continuous H_2O_2 conversion is observed, more markedly during the first 2 h, reaching 55% of conversion after 8 h. A similar furfural conversion is observed (58%), but the temporal profile indicates a faster reaction rate after 2 h. This profile is congruent with the presence of catalytic steps activated by an intermediate.

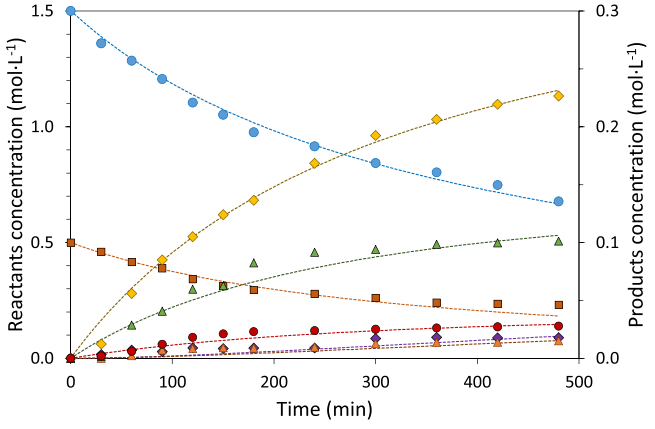

Fig. 1. Furfural oxidation with H_2O at 50 ºC in absence of a catalyst. Symbols: H_2O_2 (●); furfural (■); formic acid (◆); 2-hydroxyfuran (▲); furoic acid (●); maleic acid (◆); and 2(5 H) furanone (▲). Broken lines correspond to the kinetic model predictions.

The product distribution is congruent with previous literature, despite the diverging values because of the different temperatures used [51]. Formic acid (FA) is the main reaction product, with a clear increasing trend, yielding more than 0.2 mol·L^{-1} after 6 h. 2-Hydroxyfuran is also relevant (HF, 0.12 mol·L^{-1}), showing a typical profile of a primary compound, with an almost flat concentration after 4 h justified by its decomposition. The same trend is detected for furoic acid (FCA), although FCA is obtained with significantly lower concentrations (max. value of 0.03 mol·L^{-1}). The stable phase of HF and FCA corresponds with an increase in minority products, 2(5 H)-furanone (FN) and maleic acid (MA), suggesting that these compounds are obtained by the oxidation of one or both of these precursors (HF and FCA). Consequently, their formation is equilibrated with their decomposition. The final concentrations of FN and MA, 0.018 and 0.015 mol·L^{-1}, are too low to support a strong discussion about the mechanistic route to their formation.

The final carbon balance in the liquid phase is 85.4%, suggesting a significant carbon loss in the gas phase. The presence of any other condensated product in the liquid phase or humins was discarded considering the lack of any unknown signal on the HPLC chromatograms. Moreover, solids were not recovered after the reaction. This loss is then compatible with CO_2 released because of the total oxidation of the different compounds. A separate analysis of the gas phase by a mass-spectrometer identifies CO_2 as the only carbon-containing molecule of the gas sample.

These results suggest that formic acid (FA) is a common product obtained by all the routes that produce C4 compounds from furfural (C5). In fact, there is a good correspondence between FA concentration and the difference between the furfural converted and the furoic acid obtained (once the carbon balance closure is considered). Based on this premise, FA is excluded from the selectivity analysis (see Fig. 2), only considering the C4-C5 compounds. Thus, in carbon basis (Eq. 4), the reaction in absence of catalyst produces 60% of HF and similar selectivity of FCA (20.5%) and the mixture of FN and MA (9% and 10.5%). In global terms, these results indicate that the 2-hydroxyfuran route (Baeyer-Villiger mechanism, henceforth, B-V) prevails, the compounds of this pathway being 80% of the total mixture. It is expected that introducing an heterogeneous catalysts could modify the ratio between the two main routes of furfural partial oxidation and, subsequently, the relative distribution of products.

3.2. Influence of the catalytic support

Once the relevance of the homogeneous reaction pathways was determined, the activity of the considered bulk supports was compared. The main characterization results in terms of morphology, acidity, and basicity of the considered supports are summarized in Table 1. Data shown in this table are obtained by the analysis of N_2 physisorption isotherms, NH_3 and CO_2 spectra included in the Supplementary Information (Fig. S1-S3).

All the catalysts are mesoporous materials with surface areas from 60 (TiO_2) to 180 m^2·g^{-1} (MgAl) and pore diameters significantly higher than the kinetic diameter of all the molecules involved in the process. The absence of diffusional limitations, that could be assumed based on these data, has been theoretically corroborated, considering the Carberry number (Ca) and the Wheeler-Weisz criteria. The complete discussion is included in the Supplementary Information (Table S1). To sum up, external and internal mass transfer limitations are discarded since all the Ca and the Thiele modulus values are lower than $7 \cdot 10^{-7}$ (the limit to consider it as relevant being in 0.05) and $2 \cdot 10^{-3}$ (0.1 is the limit to being relevant). Thus, the reaction is under kinetic control and the different activity is related to the chemical surface properties, in terms of acidity and basicity, or the redox capacity, in the case of TiO_2 and CeO_2.

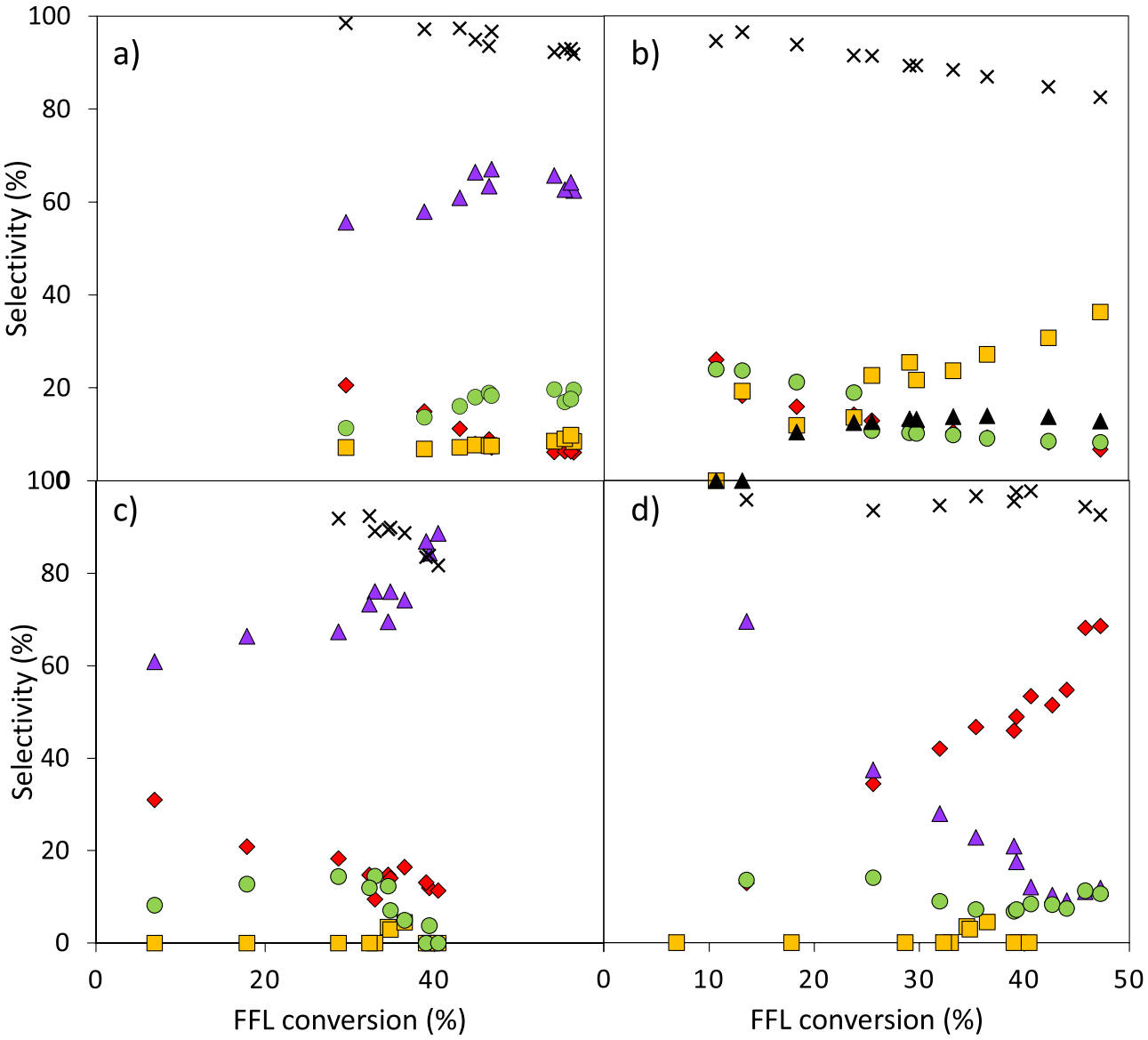

Fig. 2. Conversion - selectivity plots for furfural oxidation using H_2O_2 at 50 ºC over (a) MgAl, (b) MgZr, (c) CeO_2, and (d) TiO_2. Data correspond to carbon balance (x), and selectivities to MA (◆), FN (■), HF (▲), FCA (●), and HFN (▲).

Fig. 2 illustrates, in terms of selectivity vs. conversion, the experimental data obtained with the four metal oxides tested, keeping the temperature (50 ºC) and the initial H_2O_2/furfural ratio (3) of the homogeneous experiments described in the previous section. Results obtained with MgAl match those obtained in the absence of a catalyst, whereas the other three supports present relevant differences, including the formation of other intermediates, such as 5-hydroxy-2(5 H)furanone (HFN), β-formylacrylic acid (BFA), and malic acid (MAL). The presence of these compounds suggests that some steps of the global mechanism require a heterogeneous catalysts to be feasible.

Obtained results can be turned by the reactivity of the hydrogen peroxide. Relevant differences between materials were found, from a slight increase with MgAl and MgZr (64% and 70% at the final reaction time) to an almost total decomposition in the case of CeO_2 (93.7%), with an intermediate behaviour for the TiO_2.

Furfural conversions are lower than the one reached without a catalyst, detecting values from 33% (MgZr) to 46.7% (MgAl), with an opposite trend than the one observed for H_2O_2 conversion,. These results indicate that H_2O_2 is involved in all the steps where furfural is. Thus, the fast decrease of H_2O_2 concentration leads to a reduction in the rates of these reactions, with the subsequent reduction in the furfural conversion. This conclusion is supported by the literature. López Granados and co-workers demonstrate that the larger the H_2O_2 concentration, the faster the furfural conversion rate [22], and several authors propose using different oxides as catalysts for hydrogen peroxide decomposition [52,53].

According to the previous discussion, the H_2O_2 conversion and, subsequently, the furfural one is improved by the redox properties of Ce [54], Ti [14], and Zr [55]. However, the comparison between the blank and experiments with MgZr suggests that the role of acidic/basic properties of the catalysts in the product distribution and the reaction control cannot be discarded.

With MgAl, the distribution of the main products is quite similar than in absence of any catalyst, obtaining a final sample enriched in HF (66.6%) with 18.3% of FCA and 17% of the sum of FN, MA and HFN (catalytic route not observed with the blank). The high carbon balance

Table 1
Main characterization properties of the different supports used in this work.

	MgAl	MgZr	TiO_2	CeO_2
N_2 physisorption				
Surface area ($m^2 \cdot g^{-1}$)	179	111	59	123
Pore volume ($cm^3 \cdot g^{-1}$)	0.4	0.7	0.3	0.3
Pore diameter (nm)	7	18	19	8
Acidity (μmol $NH_3 \cdot g^{-1}$)				
Physisorbed (<100 °C)	109.6	16.3	17.4	0
Weak (100 – 200 °C)	181.5	227.0	67.3	45.7
Medium (200–400 °C)	78.5	147.4	127.7	177.3
Strong (>400 °C)	161.2	183.7	18.6	9.2
Total	*530.7*	*574.4*	*231.1*	*232.2*
Basicity (μmol $CO_2 \cdot g^{-1}$)				
Physisorbed (<100 °C)	14.2	17.9	15.6	22.5
Weak (100 – 200 °C)	40.1	50.3	0	0
Medium (200–400 °C)	0	97.2	11.3	9.5
Strong (>400 °C)	268.5	0	11.0	6.1
Total	*322.7*	*165.3*	*37.9*	*38.2*

(93%) and the constant concentration of FCA suggests a positive role of strong basic sites preventing CO_2 formation and stabilizing the resulting organic acids.

In the case of MgZr, the higher strength of the acid sites promotes B-V oxidation pathways [56], observing a significant decrease in the furoic acid selectivity (10.1%), as well as an increase in the formation of acyclic compounds (selectivity of 33.7% of BFA), and their total decomposition to CO_2, fostered by the absence of strong basic sites that could stabilize the organic acids.

With CeO_2, furoic acid is only observed in traces at the beginning of the reaction and FN, HFN, BFA or MAL are not detected. This material presents the highest production of 2-hydroxyfuran (HF), with almost constant selectivity during all the reaction (~90%). In addition to the redox activity of this catalyst, its marked medium-strength acidity (see data in Table 1), with the subsequent total H_2O_2 decomposition (only observed with this material) explains the promotion of this route. The carbon balance (83.2%) suggests that the decomposition of organic compounds is relevant. The maleic acid selectivity is not negligible (11.3%). These results are explained by the easy Ce^{3+}/Ce^{4+} redox transition, increasing the oxygen mobility and storage capacity, favoring total oxidations [57].

TiO_2 highlights by the fast decomposition of primary products, with maximum selectivities of 67.2% for HF (after 30 min), and 17.4% for FCA (after 1 h). Due to their decomposition, maleic acid represents more than 66% of the total selectivity after 8 h, result that corresponds to 20.7% of the product yield. This material presents the best carbon balance (94.8%), discarding relevant decomposition to CO_2. The acidity and basicity properties of this material cannot explain these results, its redox capacity being proposed as the main responsible of it. In the case of TiO_2, oxidations are enhanced but not the decompositions, suggesting a complex effect of support oxygen vacancies.

According to this support screening, the role of heterogeneous catalysts tuning the selectivity is very relevant, in such a way that CeO_2 is proposed for the selective production of hydroxyfuran (HF), whereas maleic acid (MA) formation is promoted with TiO_2. This analysis is not so conclusive concerning other reaction intermediates, such as furoic acid. For this compound, a maximum selectivity of 28% is obtained with MgZr, but this result corresponds to a low FFL conversion (9.2%, 1 h) and the FCA yield is then almost negligible (1.2%). On the contrary, results with MgAl present a better balance between conversion and selectivity, reaching a maximum yield of 6.7% after 6 h. To sum up, the analysis of relevant reaction intermediates requieres a balance between the catalytic activity and the reaction time to prevent the advance of the reaction to more oxidized compounds.

3.3. Kinetic study

With the temporal evolution of reactants and products obtained with and wihtout catalysts, and considering the literature [10,17,18], the mechanism shown in Scheme 1 is proposed.

According to this mechanism, furfural is oxidized by two parallel pathways, obtaining furoic acid and 2-hydroxyfuran, respectively, as primary compounds. Through the second pathway (B-V), oxidation implies a partial decomposition, releasing formic acid. 2-Hydroxyfuran is a reactive intermediate that undergoes dehydration, yielding 2(5 H) furanone. The co-presence of hydrogen peroxide and formic acid catalyzes the oxidation of furoic acid and 2(5 H)furanone into maleic and fumaric acid, two isomers in cis-trans rearrangement equilibrium. The low pH (2.8 after 8 h) and the oxidizing medium promotes the degradation of these compounds through consecutive oxidative decarboxylations, releasing CO_2 and water [6]. The absence of a direct correspondence between the products and the hydrogen peroxide conversion suggests an independent self-decomposition of this reactant.

Experimental results were fitted to the kinetic model obtained by applying the mass balances suggested by the reaction mechanism and considering the hypothesis of an ideal stirred batch reactor, according to Eq. (7) to (14). In these equations, fumaric and maleic acid are considered together. All the compounds are labeled as indicated in Scheme 1 to simplify the mathematical expressions.

$$\frac{dC_H}{dt} = -k_1 \cdot H - k_2 \cdot FFL \cdot H - k_3 \cdot FCA \cdot H - k_4 \cdot FFL \cdot H - k_6 \cdot FN \cdot H - k_7 \cdot HF \cdot H - k_8 \cdot HFN \cdot H - k_9 \cdot MA \cdot H - k_{10} \cdot MA \cdot H \quad (7)$$

$$\frac{dC_{FFL}}{dt} = -k_2 \cdot FFL \cdot H - k_4 \cdot FFL \cdot H \quad (8)$$

$$\frac{dC_{FCA}}{dt} = k_2 \cdot FFL \cdot H - k_3 \cdot FCA \cdot H \quad (9)$$

$$\frac{dC_{FA}}{dt} = k_3 \cdot FCA \cdot H + k_4 \cdot FFL \cdot H - k_9 \cdot MA \cdot H \quad (10)$$

$$\frac{dC_{MA}}{dt} = k_3 \cdot FCA \cdot H + k_6 \cdot FN \cdot H + k_8 \cdot HFN \cdot H - k_{10} \cdot MA \cdot H \quad (11)$$

$$\frac{dC_{HF}}{dt} = k_4 \cdot FFL \cdot H - k_5 \cdot HF \cdot H - k_7 \cdot FN \cdot H \quad (12)$$

$$\frac{dC_{FN}}{dt} = k_5 \cdot HF \cdot H - k_6 \cdot FN \cdot H \quad (13)$$

$$\frac{dC_{HFN}}{dt} = k_7 \cdot FN \cdot H - k_8 \cdot HFN \cdot H \quad (14)$$

The coexistence of homogeneous and heterogeneous reaction pathways is modeled considering each kinetic rate constant as the sum of two values: a constant one due to the homogeneous contribution (related to the activity of hydrogen peroxide and protons), and a variable one related to the solid catalyst. Due to the extended number of terms, this disaggregation ($k_i = k_{(i,hom)} + k_{(i,het)}$) is not specified in the equations. This methodology requires a previous analysis of the blank experiment to isolate the contribution of the homogeneous rates in those steps identified without a solid catalyst. This analysis also allows identifying those steps that require a solid catalyst to be promoted (identified with green shadow in Scheme 1).

The low pH (<3) obtained in less than 2 h allows considering the homogeneous catalysis is due to the presence of protons as constant. Based on these appreciations, the effect of the acidity is embedded in the common contribution (homogeneous terms) without including any extra term in the mass balances. Since no relevant differences between the acids that could release these protons were observed, the main contribution is attributed to formic acid because of its significantly higher

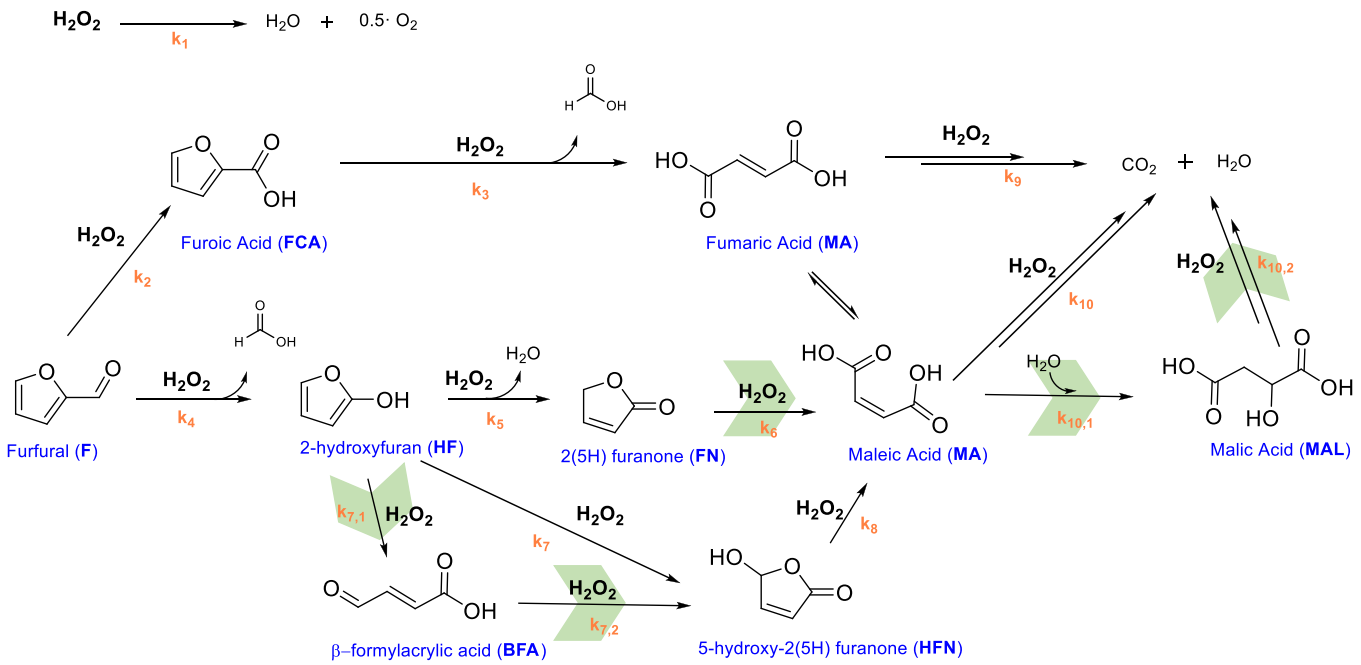

Scheme 1. Reaction network of furfural oxidation using H_2O_2 as oxidizing agent. Steps highlighted in green require a heterogeneous catalyst.

concentration (more than 90% in some cases).

In contrast, experimental results demonstrate a marked influence of the hydrogen peroxide concentration on the different steps, as well as a different evolution of its concentration as a function of the catalyst used. Therefore, it is a relevant parameter in the mass balances for the heterogeneous catalysis, leading to an apparent second order kinetics for most of the steps, as well as a decomposition rate (k_1) with a homogeneous and a heterogeneous contribution, in the same way as for the organic compounds.

The kinetic rates of the main steps (k_1-k_4) are summarized in Table 2, whereas the values for secondary steps that could be affected by a higher inaccuracy (due to the lower concentrations to be fit) are included in the Supplementary Information (Table S2). The kinetic rates reported for the different supports correspond only to the heterogeneous contribution. The real rates are obtained by the sum of both terms, but the discussion is more clearly based only on those terms affected by the solid catalysts.

The goodness of fit for the blank experiment is illustrated in Fig. 1, observing a great correspondence between experimental (dots) and fitted values (broken lines). These values represent a common homogeneous contribution for those experiments with a solid catalyst.

As illustrated in Scheme 1, when a solid catalyst is involved, the quantification of all the intermediates suggests that steps 7 and 10 of the original mechanism must be decomposed into two intermediate ones, justifying the detection of β-formylacrylic (BFA) and malic acid (MAL), compounds not detected without a catalyst. The detailed temporal profiles comparing experimental and fitted data obtained with the most promising supports (TiO_2 and MgAl) are included in Fig. 3, whereas the corresponding ones with MgZr and CeO_2 are incorporated in the Supplementary Information (Fig. S4).

The complexity of the mechanism limits the analysis based on the characterization parameters. However, a clear correspondence between the main kinetic rates and the catalyst acidity is observed, as shown in Fig. 4.

As anticipated by the literature [58,59] and corroborated with our experimental results, the lateral route of 2-hydroxyfuran formation (B-V mechanism) is promoted by the acidity (k_4), the medium-strength sites being the most relevant ones for this step. An opposite influence is observed for the furoic acid production, supporting the negative role of acidity to maximize its yield. In the same way, a positive effect of acidity is observed also for the following oxidizing steps, with a higher relevance of the strong acidic sites for the total decomposition of the two main products of the reaction, the 2-hydroxyfuran, and furoic acid, producing CO_2 as the final compound.

The parallel analysis considering the basicity of these materials is not conclusive. The lack of a clear correlation between oxidizing steps and basicity discards the prevalence of the Cannizaro disproportionation mechanism also proposed in the literature [11,60]. In good agreement, furfuryl alcohol is not observed. Although a positive role of basicity is suggested by the experimental results (increasing the acids stability and preventing their total decomposition into CO_2), the redox properties of some of these catalysts alter the H_2O_2 available to produce the furfural conversion, this fact prevailing over the basicity. These effects are more relevant for first intermediates, such as the furoic acid (FCA), compounds whose production is more sensitive to the weak equilibrium between activity, selectivity and stability.

Table 2
Reaction rate constants based on the proposed reaction network. Units: k_1 (s^{-1}); k_2 – k_4 ($L{\cdot}mol^{-1}{\cdot}s^{-1}$). Except in the case of the blank experiment, values shown correspond to the heterogeneous contribution to each step, the total rate being obtained as the sum of the homogeneous rate (blank experiment) and each value.

	Blank	MgAl	MgZr	CeO_2	TiO_2
k_1	$1.8{\cdot}10^{-5}$	0	$3.2{\cdot}10^{-5}$	$2.2{\cdot}10^{-4}$	$9.3{\cdot}10^{-6}$
k_2	$1.0{\cdot}10^{-5}$	$2.1{\cdot}10^{-5}$	$1.4{\cdot}10^{-5}$	$1.1{\cdot}10^{-5}$	$1.8{\cdot}10^{-5}$
k_3	$5.2{\cdot}10^{-5}$	$3.9{\cdot}10^{-1}$	$3.9{\cdot}10^{-1}$	$6.4{\cdot}10^{-2}$	$1.1{\cdot}10^{-1}$
k_4	$1.9{\cdot}10^{-5}$	$3.4{\cdot}10^{-6}$	$3.4{\cdot}10^{-6}$	$2.8{\cdot}10^{-5}$	$9.9{\cdot}10^{-6}$
r^2	0.914	0.909	0.903	0.919	0.931

3.4. Activity of bifunctional catalysts

Bifunctional catalysts were prepared with a theoretical 1% of Pt, Pd, or Au. These metals were chosen considering their high oxidation capacity demonstrated for similar systems [57], with the aim to analyze their influence tuning the selectivity of the reaction. The low metal loading leads to good metal dispersions, maximizing the activity of these metal particles and enabling a direct comparison with the bulk material.

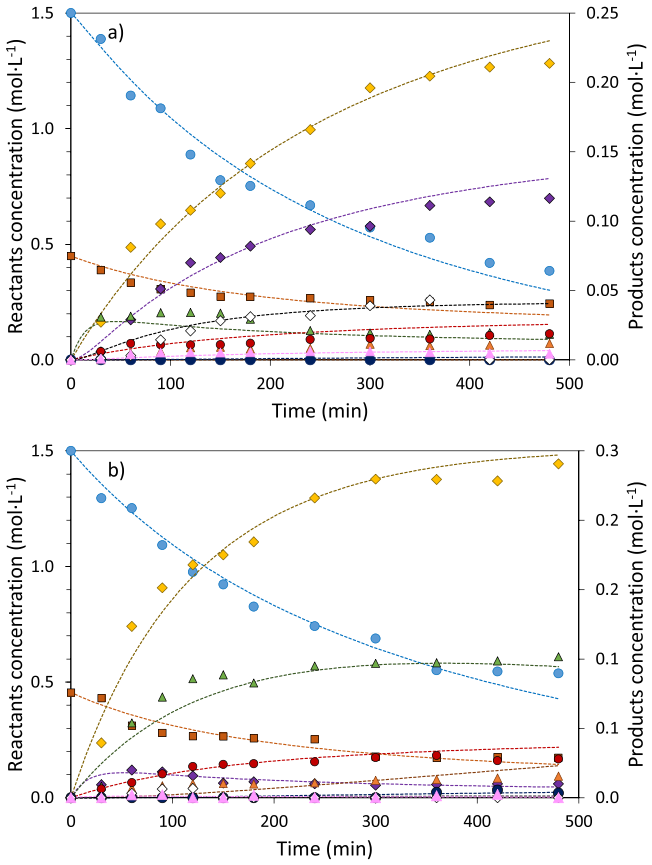

Fig. 3. Furfural oxidation with H_2O_2 at 50 ºC in presence of (a) TiO_2 and (b) MgAl. Symbols: H_2O_2 (●); FFL (■); FA (◆); HF (▲); FCA (●); MA (◆); FN (▲); HFN (●); BFA (◇); MAL (▲). Broken lines correspond to the kinetic model predictions.

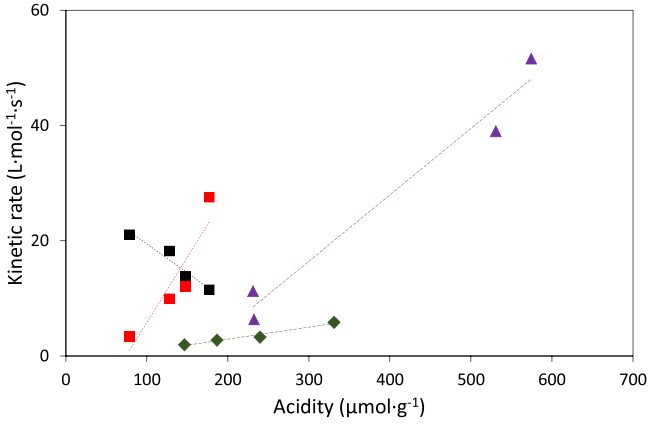

Fig. 4. Evolution of the kinetic constants for furfural conversion considering both pathways, k_2 (■, x10^{-5}) and k_4 (■, x10^{-6}), as a function of the medium-strength acidity; HF oxidation, $k_5 + k_7 + k_{11}$ (◆, x10^{-4}) as a function of the medium-strength and strong acid sites, and the furoic acid oxidation, k_3 (▲, x10^{-2}) as a function of the total acidity of the oxides used as catalysts.

In good agreement, there is a complete correspondence between the surface structure of the bulk and the metal-modified catalysts, as observed by XRD (Figure S5-S8). Table 3 shows the main characterization results, in terms of morphology, metal loading and dispersion, and surface chemistry.

Bifunctional catalysts keep the surface properties of the bulk materials, observing slight decreases in the surface area due to the non-porous surface of metal nanoparticles. The N_2 isotherms are included in the Supplementary Information (Fig. S9). Considering the preparation methodology (dry impregnation except in the case of Au materials), these particles are located inside the pores. Consequently, there is a slight increase in the average size of the pores because the smallest ones can be completely blocked, increasing the relative weight of the biggest ones. This partial blockage is also congruent with the differences observed in the surface chemistry. In most cases, the total concentration of the acid sites is lower than the one of the bulk materials, keeping the same relative weight in strength terms. The highest decrease is observed with Pt/MgAl (70.1% with respect to the total concentration of the parent material), being also very significative with Pd/TiO_2 (33.4%), Pd/TiO_2 (54.9%) and Au/TiO_2 (43.7%). For the other materials, the decrease is less relevant, in general lower than 20%. The effect on the basicity is not so clear. There is a relevant decrease in basicity with Au/TiO_2 and Pt/MgAl (~33%), whereas the basicity of other materials, such as Pt/TiO_2 and Pd/TiO_2 significantly increases. The TPD data are included in the supplementary information (Fig. S10-S11).

The dispersion values indicated in these tables correspond to TEM results. The CO chemisorption analyses were also carried out, obtaining discrepancies lower than 5% in most cases (see Table S3). However, these results were not included in these tables since this technique could not be efficiently applied to Au-catalysts. TEM results demonstrate the presence of reduced metal particles in the range of 5.5–7.5 nm, with slightly lower values for Pt/CeO_2 and Pd/CeO_2 (4.6 and 1.5 nm). These values were obtained after measuring more than 100 particles from micrographs such as those shown in the supplementary information (Fig. S12-S15). In agreement with these similar particle sizes, most of these materials have a similar metal dispersion, from 18% to 30%, reaching values up to 45% for those catalysts with the smallest particle size.

These dispersion results, as well as the own nature of these metals and their synergetic effect with the surface chemistry of the catalytic support, are assumed to be the most relevant parameters to discuss the catalytic activity of these bifunctional catalysts. TPR analyses of the spent catalysts discard that experimental results are affected by a total or partial oxidation of metal particles. As indicated in the introduction section, furoic acid (FCA), 2(5 H) furanone (FN), maleic and malic acids (MA and MAL, respectively) are the most interesting compounds obtained by the furfural partial oxidation. 2(5 H) furanone (FN) is not significantly produced with almost none of the catalysts tested, with the exception of Pt/MgZr, a catalyst that selectively produces this compound (100%).

Fig. 5 shows the FCA selectivity-conversion plots for the different catalysts, whereas main results after 8 h reaction time are summarized in Table 4 (the detailed products distribution is included in the supplementary information (Table S4). As observed in Fig. 5, the presence of noble metals increases the maximum selectivty of FCA obtained with each support. Platinum is the only exception, its behaviour strongly depending on the support. Thus, using MgZr and CeO_2, FCA is not detected whereas, with the other two oxides (MgAl and TiO_2), the maximum selectivities (40.8% and 23.3%) are reached in less than 1 h. In the case of Pt/MgAl, the corresponding FFL conversion is almost negligible (1.5%), whereas Pt/TiO_2 is significantly more active, with 18.9% of FFL conversion after this 0.5 h.

Pt/MgAl shows the slowest kinetic (9.2% of FFL conversion after 8 h), but its selectivity and stability to FCA is quite high, with a remaining selectivity of 34.8%. Both results are congruent with the significant blockage of acidic sites produced by Pt nanoparticles, slowing down all the oxidizing reactions. On the contrary, Pt/TiO_2 is discarded because of the poor FCA stability observed.

Pd/MgAl is the catalyst that produces the maximum FCA selectivity

Table 3
Main characterization properties of the different bifunctional oxides used in this work.

	Pd/MgAl	Pt/MgAl	Au/MgAl	Pd/MgZr	Pt/MgZr	Au/MgZr	Pd/CeO_2	Pt/CeO_2	Au/CeO_2	Pd/TiO_2	Pt/TiO_2	Au/TiO_2
N_2 physisorption												
Surface area ($m^2 \cdot g^{-1}$)	151	165	196	82	128	78	118	114	115	66	54	63
Pore volume ($cm^3 \cdot g^{-1}$)	0.4	0.3	0.4	0.7	0.6	0.3	0.2	0.2	0.2	0.4	0.4	0.7
Pore diameter (nm)	8.0	12.1	5.6	23.1	17.7	11.9	4.8	4.4	4.7	21.0	24.4	35.9
ICP, Metal loading (%)	0.87	0.87	1.05	0.97	0.88	0.89	0.80	0.79	1.06	0.85	0.82	1.01
TEM												
Particle size (nm)	8.3	7.7	9.9	7.8	11.9	8.6	1.5	4.6	9.3	8.5	10.8	6.5
Dispersion (%)	14.1	21.6	15.9	16.5	15.4	14.7	49.4	36.4	13.8	13.1	11.0	24.2
Acidity ($\mu mol\ NH_3 \cdot g^{-1}$)												
Physisorbed (<100 °C)	0	19.7	116.1	0	52.4	75.5	0	0	35.5	22.9	25.4	22.2
Weak (100 – 200 °C)	0	58.9	158.1	119.8	116.7	191.7	201.3	231.1	36.2	81.4	78.3	52.9
Medium (200–400 °C)	315.0	36.5	64.1	109.3	148.0	130.0	0	22.9	124.2	0	50.3	54.9
Strong (>400 °C)	50.7	43.5	0	192.3	86.3	0	0	0	0	0	0	0
Total	365.7	158.6	338.3	421.5	403.4	397.3	201.3	254.0	195.9	104.3	153.9	130.0
Basicity ($\mu mol\ CO_2 \cdot g^{-1}$)												
Physisorbed (<100 °C)	24.8	12.2	36.4	6.6	40.3	13.8	24.1	110.5	28.3	17.1	24.5	15.0
Weak (100 – 200 °C)	0	58.0	80.3	37.5	78.3	33.1	0	0	8.1	0	0	0
Medium (200–400 °C)	116.5	93.1	199.2	50.4	110.1	70.2	0.8	16.4	0	4.9	3.1	6.5
Strong (>400 °C)	156.7	56.5	0	25.9	20.9	0	4.5	37.8	14.1	46.7	38.8	3.8
Total	298.1	219.8	315.8	120.3	249.7	117.1	29.4	164.4	50.5	68.6	66.3	25.2

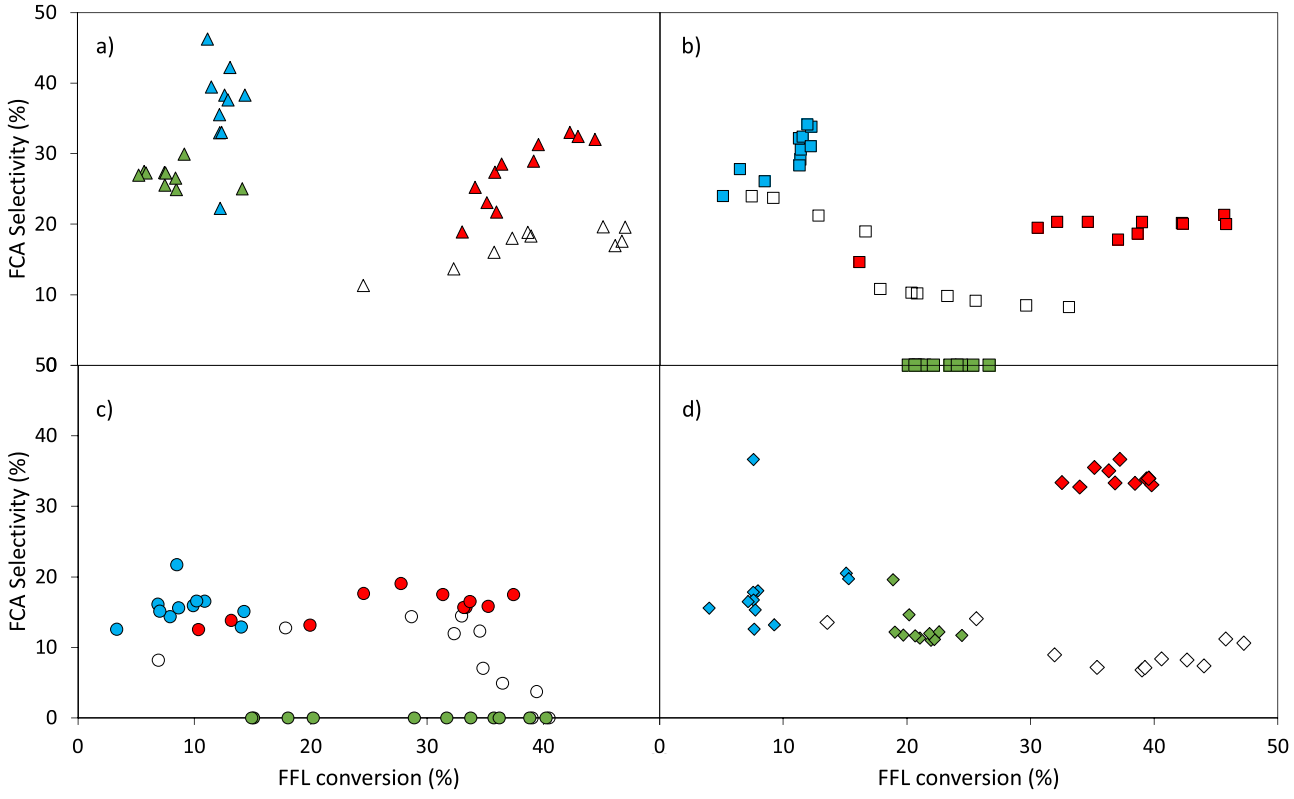

Fig. 5. Conversion vs. FCA selectivity plots for furfural oxidation using H_2O_2 at 50 °C over (a) MgAl-supported, (b) MgZr-supported, (c) CeO_2-supported, and (d) TiO_2-supported catalysts. Red dots correspond to Au-based catalysts, green dots to Pt-based catalysts, blue dots to Pd-based catalysts, and white dots to bulk supports.

(49.2% after 3 h of reaction, with a 11.2% of FFL conversion). The slow activity also observed with this material results in a quite stable FCA production (remaining selectivity after 8 h of 37.1%). Very similar results are reached with Pd/MgZr (37.1% of selectivity with 12% of FFL conversion). The FCA selectivities obtained when using supports with redox activity are significantly lower, both comparing the maximum values (22.3% and 23.3% with Pd/CeO_2 and Pt/TiO_2, respectively), and final results after 8 h.

Both using Pt and Pd, almost total H_2O_2 conversion is reached in less than 3 h (>99%), this fact strongly affecting the distribution of the

Table 4
Furfural conversion and selectivity distribution after 8 h of reaction at 50 °C as a function of the catalyst used.

	FFL Conv. (%)	Selectivity (%)			
		FCA	FN	MA	MAL
MgAl	49.2	1.8	66.6	0	0
Pd/MgAl	14.4	37.4	0	5.9	18.8
Pt/MgAl	9.2	34.8	4	3.9	10.1
Au/MgAl	49.2	37.1	2.2	17.9	0.3
MgZr	33.1	10.1	35.6	6.6	1.4
Pd/MgZr	12	37.1	0	7.7	27.5
Pt/MgZr	21.4	0	100	0	0
Au/MgZr	45.8	23.8	4	18	1.9
CeO_2	40.5	0	0	11.3	0
Pd/CeO_2	14	13.8	0	7.1	21.4
Pt/CeO_2	27.8	0	0	0	78.5
Au/CeO_2	37.4	20.9	0	5.6	0
TiO_2	45.8	13.6	6.9	66.2	2.6
Pd/TiO_2	15.3	23.0	0	76.5	0
Pt/TiO_2	22.6	14.8	6.8	9.8	7.7
Au/TiO_2	39.5	39.1	0	0	38.1

products. These results could be different modifying the reactor configuration to allow a continuous addition of H_2O_2. Despite the high interest of this configuration (previously tested in the literature [32]), the continuous change in volume limits the use of temporal data to evaluate the kinetic of the systems as well as the influence of the catalyst in the H_2O_2 decomposition rate. These points will be deeply discussed below.

Concerning the Au-modified catalysts, the maximum FCA selectivities are quite high (38.1%, 24.2%, 22.7%, and 42%, with Au/MgAl, Au/MgZr, Au/CeO_2, and Au/TiO_2, respectively). This metal offers the maximum stability of this production, and their final FFL conversion are the highest ones (from 37 to almost 50%), resulting in the maximum FCA yields obtained with all the screening of catalysts tested in this work (8.5%, 7.5% and 7.1% with Au/MgAl, Au/MgZr, and Au/TiO_2). These yields could be significantly increased by modifying the reaction configuration since FFL conversion increases by increasing the catalytic loading or recycling the unconverted reactant. Thus, the relevance of these results is directly related to the high selectivity obtained. Concerning to H_2O_2, although obtained conversions are very high (86.6%, 97.1%, 81.1%, and 97.3%, with Au/MgAl, Au/MgZr, Au/CeO_2, and Au/TiO_2 after 8 h), a remaining amount of oxidant is present in most of the experiments. In the same way, final carbon balances are always higher than 86% (see Table S4), the lack of information because of total FFL decomposition into CO_2 being not very relevant. The similar trends obtained with all the Au-modified catalysts suggests a positive role of this metal that can be discussed independently of the properties of the support (it will be analysed below). Based on these results, Au/TiO_2 is defined as the optimum catalyst to produce FCA.

The presence of noble metals also modifies the selectivity to lineal carboxylic acids, as β-formyl-acrylic (BFA), maleic (MA) and malic (MAL) acids productions. The maximum selectivities with the corresponding FFL conversions are compared in Fig. 6.

Maleic acid (MA) is produced with almost total selectivity using Pd/TiO_2 (84.8%), value reached after 5 h that corresponds to a very low FFL conversion (7.7%). The low basicity of this material suggests a low stabilization of previous intermediates, promoting their oxidation. In this case, the chemical properties seem to be more relevant than the own activity of the metal, observing the poor results obtained when using other supports.

The maximum selectivities obtained with Au/MgAl and Au/MgZr are also quite relevant (43.9% and 46.9%), but the stability of MA with these materials is very weak, suffering a fast disappearance, discarding the gold as a good metal to obtain this compound. Pt is also discarded, observing that this metal hinders the MA route.

Maleic acid (MAL) is a very unstable product that suffers fast oxidation with almost all the catalyst. Pt/CeO_2 is the only exception,

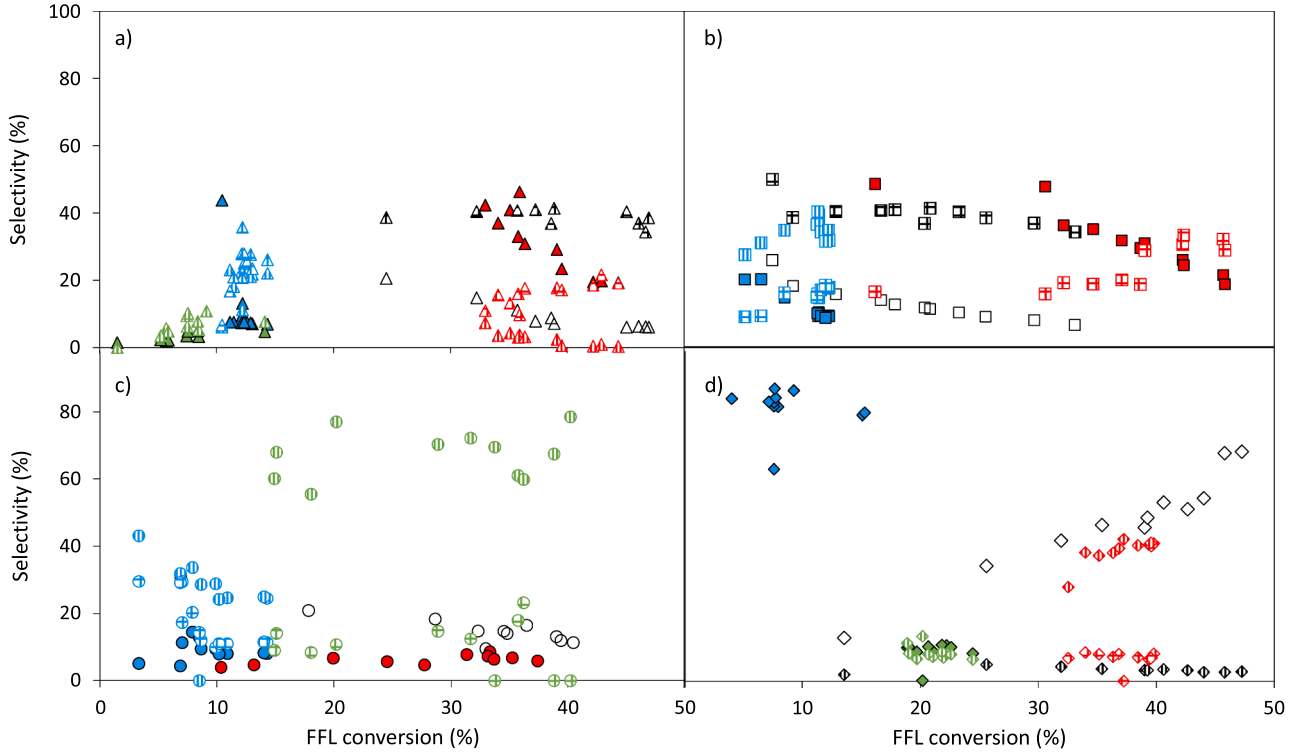

Fig. 6. Conversion vs. selectivity plots for furfural oxidation using H_2O_2 at 50 °C over (a) MgAl-supported, (b) MgZr-supported, (c) CeO_2-supported, and (d) TiO_2-supported catalysts. Red dots correspond to Au-based catalysts, green dots to Pt-based catalysts, blue dots to Pd-based catalysts, and white dots to bulk supports. Solid colors correspond to MA, vertically stripped symbols to MAL and squared symbos to BFA.

with a constant MAL production, reaching a final selectivity of 78.5% with almost 28% of FFL conversion. This result could be a synergetic effect of its low basicity (the lowest basicity of all the catalysts tested) and a particular interaction between Pt nanoparticles and the redox surface of CeO_2.

The analysis about the non-carboxylic intermediates is included in the supplementary information (Fig. S16).

3.5. Kinetic study of bifunctional catalysts

All the experimental data were fitted to the proposed kinetic model. The kinetic rates obtained for the heterogeneous contribution are summarized in Table S5 and S6. The correspondence between experimental and fitted values of the best catalysts is shown in Fig. 7, whereas the other materials are included in the Supplementary Information (Fig. S17-S20).

The main conclusions derived from the kinetic study are analyzed in Fig. 8. Except in the case of using CeO_2, all the metal modified materials show higher k_1 values than the parent supports, in good agreement with the higher hydrogen peroxide conversions obtained. The lack of correspondence between the medium-strength acidity and these values suggests the prevalence of the metal activity in the H_2O_2 decomposition over the support one. The positive role of these metals in promoting hydrogen peroxide decomposition has been previously proposed in the literature [54,61].

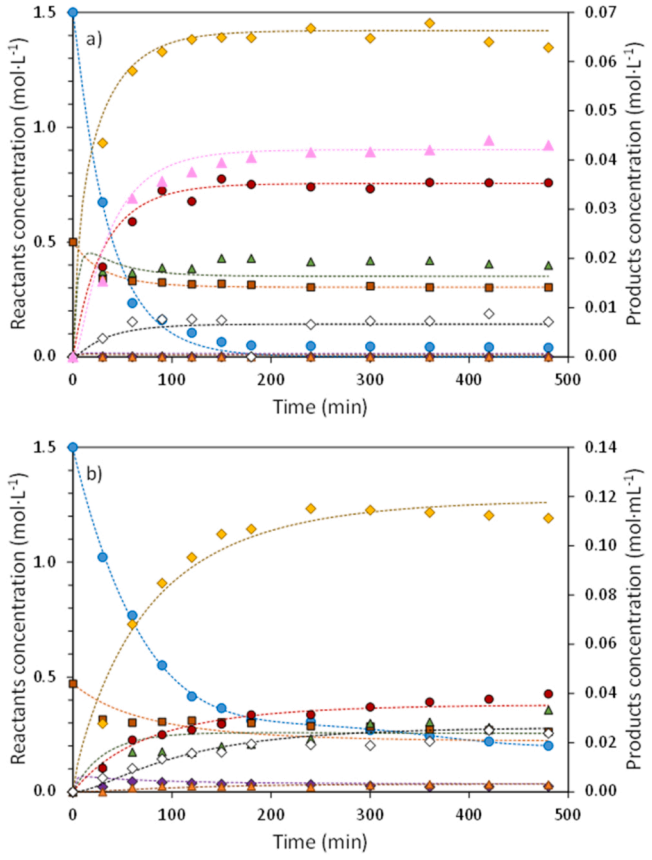

Fig. 7. Furfural oxidation with H_2O_2 at 50 ºC in presence of (a) Au/TiO_2 and (b) Au/MgAl. Symbols: H_2O_2 (●); FFL (■); FA (◆); HF (▲); FCA (●); MA (◆); FN (▲); HFN (●); BFA (◇); MAL (▲). Broken lines correspond to the kinetic model predictions.

The increment in the H_2O_2 self-decomposition is more notorious than the increase in the rates of the two first steps of the main process, as illustrated in Fig. 8a. This effect is more relevant in those catalysts involving Pd and Pt, whereas this undesired effect is less significant when using Au-modified materials. The presence of metal nanoparticles also affects the dominant oxidizing route. A high prevalence for the furoic route is observed with Pt and Au. In the case of Pt materials, this improvement requires support with redox properties, TiO_2 or CeO_2. On the contrary, the enhancement with Au is observed despite the type of support used, being more significant with mixed oxides (four orders of magnitude) because, with oxides, both steps are promoted, reducing the relative differences.

The effect of using bifunctional catalysts is extended to the undesired oxidations, the different steps that decompose the two primary compounds (FCA and HF), reducing the selectivity and the carbon balance. As observed in Fig. 8c, the relative weight of the FCA decomposition decreases, increasing the relative k_2/k_3 value. This effect is more relevant with Au materials, mainly Au/TiO_2 and Au/MgAl. As to the secondary steps, Au is the only metal that does not produce an increment in these rates (Fig. 8d). The sum of all these secondary kinetic rates is significantly higher with materials containing Pd and Pt, whereas these rates globally decrease with Au-modified catalysts to obtain values lower than those reached with the bulk materials.

These results suggest the coexistence of two different oxidizing mechanisms, the effect of metal nanoparticles (mainly Au) promoting the oxidation by a redox reaction, i.e., the furoic acid production by a selective interaction between furfural and hydrogen peroxide. On the other hand, those oxidation steps that follow a decomposition mechanism, releasing a formic acid molecule are not promoted by these bifunctional catalysts. This hypothesis suggests that the metal particles (mainly Au ones) enhance the simultaneous chemisorption of both reactants required. Thus, the decomposition of H_2O_2 occurs close to the active site where the furfural is adsorbed. On the contrary, the decomposition reactions are less selective and not as sensitive to this proximity as the furoic acid (FCA).

Au is identified as the best metal to maximize FCA production, and the metal dispersion is the most relevant parameter since this determines the frequency of the correct interactions between the active site and the reactants. This hypothesis is corroborated in Fig. 9, where a clear correspondence between the principal kinetic rates and the metal dispersion is observed. Not only the desired step (k_2) is promoted by a high dispersion, but also the hydrogen peroxide decomposition (k_1), the furoic acid decomposition (k_3), and the undesired 2-hydroxyfuran formation (k_4). These last two steps are less influenced than k_1 and k_2, in agreement with the lower slope of their correlations. Thus, a medium metal dispersion must be considered, trying to reach a selective activation of the target route. Based on this premise, an intermediate dispersion (15–20%) is defined as the optimum one, a range involving Au/TiO_2 and Au/MgAl. A similar analysis with the other metals is not conclusive, no trends for the metal dispersion being observed. This fact reinforces the hypothesis of effective chemisorption required to promote the reaction (sensitive phenomenon).

4. Conclusions

The partial oxidation of furfural using H_2O_2 is a complex reaction in which the conversion and the selectivities are defined by a combination of homogeneous and heterogeneous contributions, including acidity (to promote the oxidation), basicity (to stabilize the organic acids preventing their total decomposition into CO_2), the particular activity of each metal used (Pd, Pt or Au) and a synergetic effect between the metal and the support, mainly when the support has redox properties.

A different balance between these properties and the requirements for each step of the reaction allow proposing an optimum catalyst for each interesting compound. Thus, the 2(5 H) furanone is selectively produced with Pt/MgZr (100%), maleic acid is enhanced by using Pd/

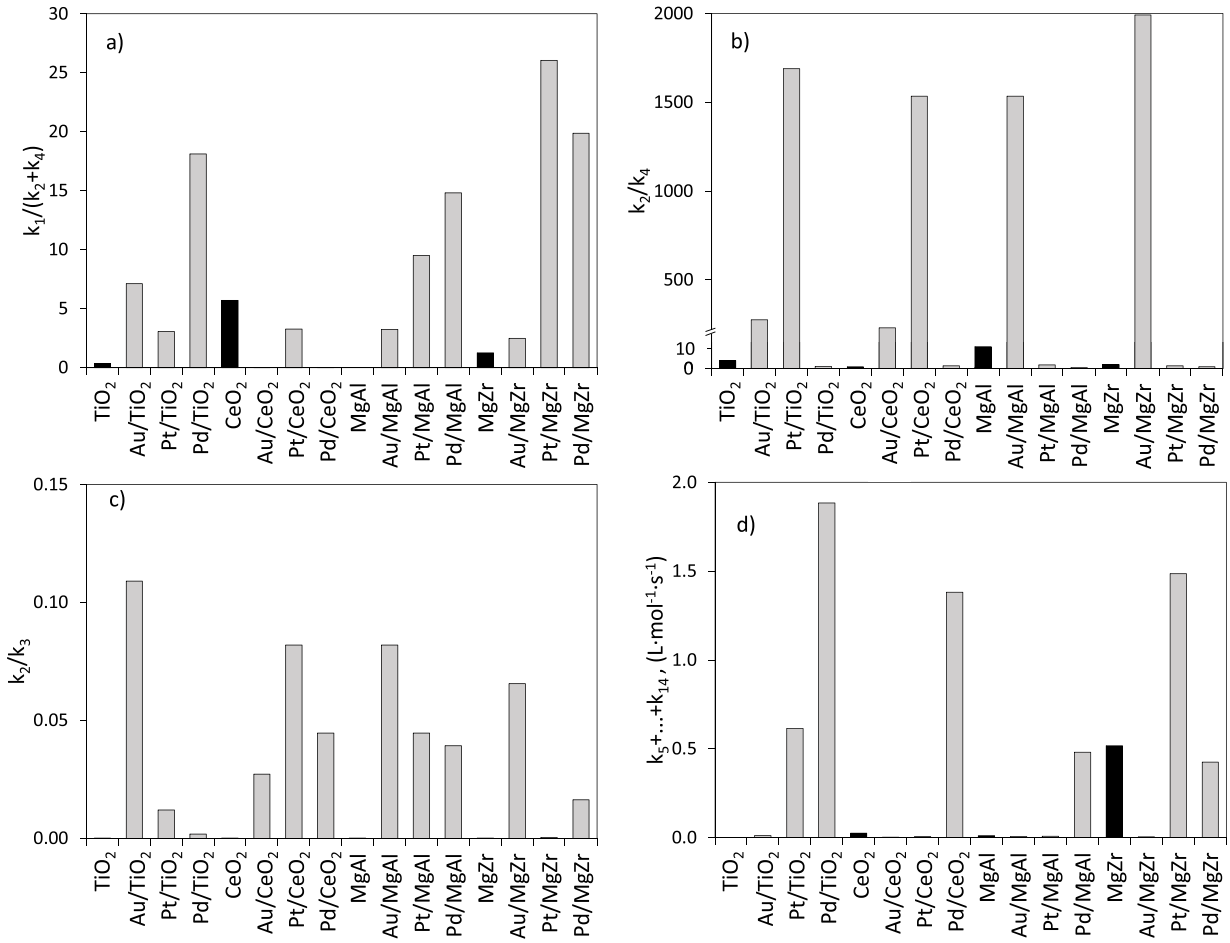

Fig. 8. : Analysis of the kinetic rates as a function of the metal-modified catalyst used.

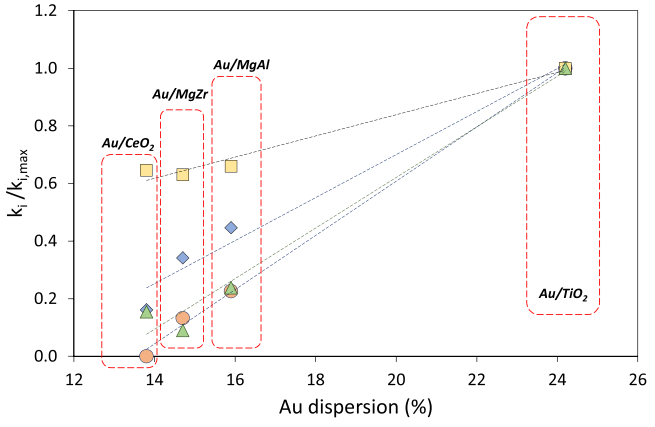

Fig. 9. Normalized evolution of k_1 (●), k_2 (◆), k_3 (■), and k_4 (▲) kinetic rates as a function of the metal dispersion of Au-modified materials. *Values obtained with Au/TiO_2 are used as reference values.*

TiO_2 (with a stable selectivity of 76.5%), and a 78.5% of selectivity to malic acid is reached with Pt/CeO_2.

As to furoic acid, the maximum selectivity is obtained with Au/TiO_2 (42%). In terms of product yields, Au/MgAl (8.5%) is also a good candidate for its production. The hypothesis that furoic acid is promoted by Au with a secondary role of the support was corroborated, defining and optimum particulate size of 5–7 nm. This size promotes the required chemisorption of furfural and hydrogen peroxide on the metal particles, reducing the relevance of the parallel reactions (the B-V mechanism).

CRediT authorship contribution statement

Paula Rapado: Investigation, Data curation, Writing – original draft. **Laura Faba:** Methodology, Formal analysis, Writing – review & editing, Supervision. **Salvador Ordóñez:** Conceptualization, Writing – review & editing, Supervision, Funding acquisition.

Declaration of Competing Interest

The authors declare that they have no known competing financial interests or personal relationships that could have appeared to influence the work reported in this paper.

Data Availability

Data will be made available on request.

Acknowledgments

This study has been financial supported by the Ministry for Science and Innovation (PID2020–112587RB-I00). The authors acknowledge the Electronic Transmission Microscope Service of University of Cantabria. Paula Rapado acknowledges to the University of Oviedo the financial support of her PhD (PAPI-21-PF-19).

Electronic supplementary material

E-supplementary data for this work can be found in e-version of this paper online.

Appendix A. Supporting information

Supplementary data associated with this article can be found in the online version at doi:10.1016/j.jece.2023.111466.

References

[1] J. Blanco-Cejas, S. Martín, M. Linares, J. Iglesias, J. Moreno, Life cycle assessment applied to bio-based platform molecules: critical review of methodological practices, J. Clean. Prod. 414 (2023), 137513, https://doi.org/10.1016/j.jclepro.2023.137513.

[2] S. Takkellapati, T. Li, M.A. González, An overview of biorefinery-derived platform chemicals from a cellulose and hemicellulose biorefinery, Clean. Technol. Environ. Policy (7) (2018) 1615–1630, https://doi.org/10.1007/s10098-018-1568-5.

[3] E. Nzediegwu, M. Pérez-Venegas, K. Auclair, M.J. Dumont, Semisynthetic production of hydroxymethylfurfural and furfural: the benefits of an integrated approach, J. Env. Chem. Eng. 10 (2022), 108515, https://doi.org/10.1016/j.jece.2022.108515.

[4] T.W. Zhang, W.Z. Li, H.N. Xiao, Y.C. Jin, S.F. Wu, Recent progress in direct production of furfural from lignocellulosic residues and hemicellulose, Bioresour. Technol. 354 (2022), 127126, https://doi.org/10.1016/j.biortech.2022.127126.

[5] P. Rapado, L. Faba, S. Ordóñez, Influence of delignification and reaction conditions in the aqueous phase transformation of lignocellulosic biomass to platform molecules, Biores. Technol. 321 (2021), 124500, https://doi.org/10.1016/j.biortech.2020.124500.

[6] F. Saleem, P. Müller, K. Eränen, J. Warnå, D. Yu Murzin, T. Salmi, Kinetics and modelling of furfural oxidation with hydrogen peroxide over a fibrous heterogeneous catalyst: effect of reaction parameters on yields of succinic acid, J. Chem. Technol. Biotechnol. 92 (2017) 2206–2220, https://doi.org/10.1002/jctb.5248.

[7] N.K. Gupta, A. Fukuoka, K. Nakajima, Metal-free and selective oxidation of furfural to furoic acid with an N-heterocyclic carbene catalyst, ACS Sust. Chem. Eng. 6 (2018) 3434–3442, https://doi.org/10.1021/acssuschemeng.7b03681.

[8] P.L. Arias, J.A. Cecilia, I. Gandarias, J. Iglesias, M.L. Granados, R. Mariscal, G. Morales, R. Moreno-Tost, P. Maireles-Torres, Oxidation of lignocellulosic platform molecules to value-added chemicals using heterogeneous catalytic technologies, Catal. Sci. Technol. 10 (2020) 271–2757, https://doi.org/10.1039/d0cy00240b.

[9] F. Drault, Y. Snoussi, S. Paul, I. Itabaiana Jr., R. Wojcieszak, Recent advances in carboxylation of furoic acid into 2,5-furandicarboxylic acid: pathways towards bio-based polymers, ChemSusChem 13 (2020) 5164–5172, https://doi.org/10.1002/cssc.202001393.

[10] G. Papanikolaou, P. Lanzafame, S. Perathoner, G. Centi, D. Cozza, G. Giorgianni, M. Migliori, G. Giordano, High performance of Au/ZTC based catalysts for the selective oxidation of bio-derivative furfural to 2-furoic acid, Catal. Commun. 149 (2021), 106234, https://doi.org/10.1016/j.catcom.2020.106234.

[11] M. Douthwaite, X. Huang, S. Iqbal, P.J. Miedziak, G.L. Brett, S.A. Kondrat, J. K. Edwards, M. Sankar, D.W. Knight, D. Bethell, G.J. Hutchings, The controlled catalytic oxidation of furfural to furoic acid using AuPd/Mg(OH)$_2$, Catal. Sci. Technol. 7 (2017) 5284–5293, https://doi.org/10.1039/C7CY01025G.

[12] Q. Tian, D. Shi, Y. Sha, CuO and Ag$_2$O/CuO catalyzed oxidation of aldehydes to the corresponding carboxylic acids by molecular oxygen, Molecules 13 (2008) 948–957, https://doi.org/10.3390/molecules13040948.

[13] F. Nocito, N. Ditaranto, D. Linsalata, M. Naschetti, R. Comparelli, M. Aresta, A. Dibenedetto, Selective aerobic oxidation of furfural into furoic acid over a highly recyclable MnO$_2$@CeO$_2$ core-shell oxide: the role of the morphology of the catalyst, ACS Sust. Chem. Eng. 10 (2022) 8615–8623, https://doi.org/10.1021/acssuschemeng.2c02341.

[14] C.P. Ferraz, S. Navarro-Jaen, L.M. Rossi, F. Dumeignil, M.N. Ghazzal, R. Wojcieskaz, Enhancing the activity of gold supported catalysts by oxide coating: towards efficient oxidations, Green. Chem. 23 (2021) 8453–8457, https://doi.org/10.1039/d1gc02889h.

[15] A. Roselli, Y. Carvalho, F. Dumeignil, F. Cavani, S. Paul, R. Wojcieszak, Liquid phase furfural oxidation under uncontrolled pH in batch and flow conditions: the role of in situ formed base, Catalysts 10 (2020) 73, https://doi.org/10.3390/catal10010073.

[16] S. Eaimsumang, S. Wongkasemjit, S. Pongstabodee, S.M. Smith, S. Ratanawilai, N. Chollacoop, A. Luengnaruemitchai, Effect of synthesis time on morphology of CeO$_2$ nanoparticles and Au/CeO$_2$ and their activity in oxidative steam reforming of methanol, J. Rare Earth 37 (2019) 819–828, https://doi.org/10.1016/j.jre.2018.11.010.

[17] R. Ciriminna, L. Albanese, F. Meneguzzo, M. Pagliaro, Hydrogen peroxide: a key chemical for today's sustainable development, ChemSusChem 9 (2016) 3374–3381, https://doi.org/10.1002/cssc.201600895.

[18] D.Y. Murzin, E. Bertrand, P. Tolvanen, S. Devyatkov, J. Rahkila, K. Eränen, J. Wärnå, T. Salmi, Heterogeneous catalytic oxidation of furfural with hydrogen peroxide over sulfated zirconia, Ind. Eng. Chem. Res. 59 (2020) 13516–13527, https://doi.org/10.1021/acs.iecr.0c02566.

[19] Y. Ni, Z.H. Bi, H. Su, L.F. Yan, Deep eutectic solvent (DES) as both solvent and catalyst for oxidation of furfural to maleic acid and fumaric acid, Green. Chem. 21 (2019) 1075–1079, https://doi.org/10.1039/c8gc04022b.

[20] M. Rezaei, A.N. Chermahini, H.A. Dabbagh, M. Saraji, A. Shahvar, Furfural oxidation to maleic acid with H_2O_2 by using vanadyl pyrophosphate and zirconium pyrophosphate supported on well-ordered mesoporous KIT-6,, J. Environ. Chem. Eng. 7 (2019), 102855, https://doi.org/10.1016/j.jece.2018.102855.

[21] C.V. Nguyen, J.R. Boo, C.H. Liu, T. Ahamad, S.M. Alshehri, B.M. Matsagar, K.C. W. Wu, Oxidation of biomass-derive furans to maleic acid over nitrogen-doped carbon catalysts under acid-free conditions. Catal. Sci. Technol. 10 (2020) 1498–1506, https://doi.org/10.1039/c9cy02364j.

[22] N. Alonso-Fagúndez, I. Agirrezabal-Telleria, P.L. Arias, J.L.G. Fierro, R. Mariscal, M.L. Granados, Aqueous-phase catalytic oxidation of furfural with H_2O_2: high yield of maleic acid by using titanium silicalite-1, RSC Adv. 4 (2014) 54960–54972, https://doi.org/10.1039/C4RA11563E.

[23] N. Ayoub, J. Toufaily, E. Guénin, G. Enderlin, Catalyst-free process for oxidation of furfural to maleic acid by high frequency ultrasonic activation, Gren Chem. 24 (2022) 4164–4173, https://doi.org/10.1039/d2gc01239a.

[24] H.F. Zhang, S.L. Wang, H.X. Zhang, J.H. Clark, F.H. Cao, A biomass-derived metal-free catalyst doped with phosphorus for highly efficient and selective oxidation of furfural into maleic acid, Green. Chem. 23 (2021) 1370–1381, https://doi.org/10.1039/d0gc04205f.

[25] A.C. Alba-Rubio, J.L.G. Fierro, L. León-Reina, R. Mariscal, J.A. Dumesic, Oxidation of furfural in aqueous H2O2 catalysed by titanium silicalite: deactivation processes and role of extraframewok Ti oxides, Appl. Catal. B 202 (2017) 269–280, https://doi.org/10.1016/j.apcatb.2016.09.025.

[26] Q. Yu, R.X. Bai, F. Wang, Q.H. Zhang, Y. Zhang, L. Qin, Z.M. Wang, Z.H. Yuan, A sustainable system for maleic acid synthesis from biomass-derived sugar, J. Chem. Technol. Biotechnol. 95 (2020) 751–757, https://doi.org/10.1002/jctb.6260.

[27] W. Zhu, F. Tao, S. Chen, M. Li, Y. Yang, G. Lv, Efficient oxidative transformation of furfural into succinic acid over acidic metal-free graphene oxide, ACS Sust. Chem. Eng. 7 (2019) 296–305, https://doi.org/10.1021/acssuschemeng.8b03373.

[28] Y.N. Palai, A. Bhrotri, A. Fukuoka, Selective oxidation of furfural to succinic acid over Lewis acidic Sn-beta, ACS Catal. 12 (2022) 3534–3542, https://doi.org/10.1021/acscatal.1c05348.

[29] H. Choudhary, S. Nishimura, K. Ebitani, Metal-free oxidative synthesis of succinic acid from biomass-derived compounds using a solid acid catalyst with hydrogen peroxide, Appl. Catal. A 458 (2013) 55–62, https://doi.org/10.1016/j.apcata.2013.03.033.

[30] V. Zvarych, A. Nakonechna, M. Marchenko, O. Khudyi, V. Lubenets, L. Khuda, O. Kushniryk, V. Novikov, Hydrogen peroxide oxygenation of furan-2-carbaldehyde via an easy, green method, J. Agric. Food Chem. 67 (2019) 3114–3117, https://doi.org/10.1021/acs.jafc.8b06284.

[31] X.M. Xiang, B. Zhang, G.Q. Ding, J.L. Cui, H.Y. Zheng, Y.L. Zhu, The effect of Mg (OH)2 on furfural oxidation with H2O2, Catal. Commun. 86 (2016) 41–45, https://doi.org/10.1016/j.catcom.2016.08.013.

[32] X. Li, X. Lan, T. Wang, Selective oxidation of furfural in a bi-phasic system with homogeneous acid catalyst, Catal. Today 276 (2016) 97–104, https://doi.org/10.1016/j.cattod.2015.11.036.

[33] J. Thuriot-Roukos, R. Khadraoui, S. Paul, R. Wojcieszak, Raman spectroscopy applied to monitor furfural liquid-phase oxidation catalyzed by supported gold particles, ACS Ometa 5 (2020) 14283–14290, https://doi.org/10.1021/acsomega.0c00091.

[34] S. Mulk, M. Sajid, L. Wang, F. Liu, G. Pan, Catalytic conversion of sucrose to 5-hydroxymethylfurfural in green aqueous and organic medium, J. Environ. Chem. Eng. 10 (2022), 106613, https://doi.org/10.1016/j.jece.2021.106613.

[35] N.D. Shcherban, R.Y. Barakov, S.A. Sergiienko, K. Eränen, J. Wärnå, D.Y. Murzin, Furfural oxidation with hydrogen peroxide over ZSM-5 based micro-mesoporous aluminosilicates, Catal. Lett. 152 (2022) 2920–2932, https://doi.org/10.1007/s10562-021-03899-9.

[36] C. Ampelli, G. Centi, C. Genovese, G. Papanikolaou, R. Pizzi, S. Perathoner, R. J. van Putten, K.J.P. Schouten, A.C. Gluhoi, J.C. van der Waal, A comparative catalyst evaluation for the selective oxidative esterification of furfural, Top. Catal. 59 (2016) 1659–1667, https://doi.org/10.1007/s11244-016-0675-y.

[37] J.T. Pirmohamed, J.M. Dowding, S. Singh, B. Wasserman, E. Heckert, A. S. Karakoti, J.E.S. King, S. Seal, W.T. Self, Nanoceria exhibit redox state-dependent catalase mimetic activity, Chem. Commun. 46 (2010) 2736–2738, https://doi.org/10.1039/B922024K.

[38] A. Lolli, R. Amadori, C. Lucarelli, M.Giorgia Cutrufello, E. Rombi, F. Cavani, S. Albonetti, Hard-template preparation of Au/CeO$_2$ mesostructured catalysts and their activity for the selective oxidation of 5-hydroxymethylfurfural to 2,5-furan-dicarboxylic acid, Microporous Mesoporous Mater. 226 (2016) 466–475, https://doi.org/10.1016/j.micromeso.2016.02.014.

[39] O. Casanova, S. Iborra, A. Corma, Biomass into chemicals: aerobic oxidation of 5-Hydroxymethyl-2-furfural into 2,5-Furandicarboxylic acid with gold nanoparticle catalysts, ChemSusChem 2 (2009) 1138–1144, https://doi.org/10.1002/cssc.200900137.

[40] T. Xie, S. Yue, T. Su, M. Song, W. Xu, Y. Xiao, Z. Yang, C. Len, D. Zhao, High selective oxidation of 5-hydroxymethyl furfural to 5-hydroxymethyl-2-furan carboxylic acid using Ag-TiO$_2$, Mol. Catal. 525 (2022), 112353, https://doi.org/10.1016/j.mcat.2022.112353.

[41] Y. Cao, X. Liu, S. Iqbal, P.J. Miedziak, J.K. Edwards, R.D. Amstrong, D.J. Morgan, J. Wang, G.J. Hutchings, Base-free oxidation of glucose to gluconic acid using

supported gold catalysts, Catal. Sci. Technol. 6 (2016) 107–117, https://doi.org/10.1039/C5CY00732A.
[42] Y.Y. Gorbanev, S. Kegnaes, A. Riisager, Effect of support in heterogeneous ruthenium catalysts used for the selective aerobic oxidation of HMF in water, Top. Catal. 54 (2011) 1318–1324, https://doi.org/10.1007/s11244-011-9754-2.
[43] F. Nocito, M. Ventura, M. Aresta, A. Dibenedetto, Selective oxidation of 5-(hydroxymethyl)furfural to DFF using water as solvent and oxygen as oxidant with earth-crust-abundant mixed oxides, ACS Omega 3 (2018) 18724–18729, https://doi.org/10.1021/acsomega.8b02839.
[44] L. Faba, E. Díaz, S. Ordóñez, Aqueous-phase furfural-acetone aldol condensation over basic mixed oxides, Appl. Catal. B 113 (2012) 201–211, https://doi.org/10.1016/j.apcatb.2011.11.039.
[45] R. López-Asensio, J.A. Cecilia-Buenestado, C. Herrera-Delgado, M.A. Larrubia-Vargas, C. García-Sancho, P.J. Maireles-Torres, R. Moreno-Tost, Mixed oxides derived from Hydrotalcites Mg/Al active in the catalytic transfer hydrogenation of furfural to furfuryl alcohol, Catalysts 13 (2023) 45, https://doi.org/10.3390/catal13010045.
[46] J. Quesada, R. Arreola-Sánchez, L. Faba, E. Díaz, V.M. Rentería-Tapia, S. Ordóñez, Effect of Au nanoparticles on the activity of TiO_2 for ethanol upgrading reactions, Appl. Catal. A 551 (2018) 23–33, https://doi.org/10.1016/j.apcata.2017.12.004.
[47] L. Faba, J. Cueto, M.A. Portillo, A.L. Villanueva Perales, S. Ordóñez, F. Vidal-Barrero, Effect of catalyst surface chemistry and metal promotion on the liquid-phase ethanol condensation to higher alcohols, Appl. Catal. A 643 (2022), 118783, https://doi.org/10.1016/j.apcata.2022.118783.
[48] J. Mazarío, Z. Raad, P. Concepción, C. Cerdá-Moreno, M.E. Domine, Pd supported on mixed oxide as an efficient catalyst for the reductive amination of bio-derived acetol to 2-methylpiperazine, Catal. Sci. Technol. 10 (2020) 8049–8063, https://doi.org/10.1039/d0cy01423k.
[49] R. Malathi, R.:P. Viswanath, Citral hydrogenation on supported platinum catalysts, Appl. Catal. A 208 (2001) 323–327, https://doi.org/10.1016/s0926-860x(00)00715-8.
[50] R. Zanella, S. Giorgio, X.-H. Shin, C.R. Henry, C. Louis, Characterization and reactivity in CO oxidation of gold nanoparticles supported on TiO2 prepared by deposition-precipitation with NaOH and urea, J. Catal. 222 (2004) 357–367, https://doi.org/10.1016/j.cat.2003.11.005.
[51] C.M. Pichler, M.G. Al-Shaal, D. Gu, H. Joshi, W. Ciptonugroho, F. Schüth, Ruthenium supported on high-surface-area zirconia as an efficient catalyst for the base-free oxidation of 5-Hydroxymethylfurfural to 2,5-Furandicarboxylic Acid, ChemSusChem 11 (2018) 2083–2090, https://doi.org/10.1002/cssc.201800448.
[52] M.A. Hasnat, M.M. Rahman, S.M. Borhanuddin, A. Siddiqua, N.M. Bahadur, M. R. Karim, Efficient hydrogen peroxide decomposition on bimetallic Pt–Pd surfaces, Catal. Commun. 12 (2010) 286–291, https://doi.org/10.1016/j.catcom.2010.10.001.
[53] H. Yang, T. Zhang, H. Tian, J. Tang, D. Xu, W. Yang, L. Lin, Effect of Sr substitution on catalytic activity of $La_{1-x}Sr_xMnO_3$ ($0 \leq x \leq 0.8$) perovskite-type oxides for catalytic decomposition of hydrogen peroxide, React. Kinet. Catal. Lett. 73 (2001) 311–316, https://doi.org/10.1023/A:1014115508872.
[54] B. Geng, S. Zhang, X. Yang, W. Shi, P. Li, D. Pan, L. Shen, $Cu_{2-x}O@TiO_2$-y Z-scheme heterojunctions for sonodynamic-chemodynamic combined tumor eradication, Chem. Eng. J. 435 (2022), 134777, https://doi.org/10.1016/j.cej.2022.134777.
[55] G. Chen, D. Hong, H. Xia, W. Sun, S. Shao, B. Gong, S. Wang, J. Wu, X. Wang, Q. Dai, Amorphous and homogeneously Zr-doped MnOx with enhanced acid and redox properties for catalytic oxidation of 1,2-Dichloroethane, Chem. Eng. J. 428 (2022), 131067, https://doi.org/10.1016/j.cej.2021.131067.
[56] C. Jiménez-Sanchidrián, J.R. Ruiz, The baeyer–villiger reaction on heterogeneous catalysts, Tetrahedron (9) (2008) 2011–2026, https://doi.org/10.1016/j.tet.2007.11.024.
[57] D. Zhao, T. Su, Y. Wang, R.S. Varma, C. Len, Recent advances in catalytic oxidation of 5-hydroxymethylfurfural, Mol. Catal. 495 (2020), 111133, https://doi.org/10.1016/j.mcat.2020.111133.
[58] H. Kumar, M.W. Fraaije, Conversion of furans by baeyer-villiger monooxygenases, Catalysts 7 (2017), https://doi.org/10.3390/catal7060179.
[59] J. Luo, H. Yuan, H. Liu, J. Li, Y. Wang, Y. Wang, J. Yao, H. Li, One-pot Baeyer–Villiger oxidation of cyclohexanone with in situ generated hydrogen peroxide over Sn-Beta zeolites, Green. Chem. Eng. 2 (2021) 294–300, https://doi.org/10.1016/j.gce.2021.03.003.
[60] C. Jiménez-Sanchidrián, J.M. Hidalgo, R. Llamas, J.R. Ruiz, Baeyer–Villiger oxidation of cyclohexanone with hydrogen peroxide/benzonitrile over hydrotalcites as catalysts, Appl. Catal. A 312 (2006) 86–94, https://doi.org/10.1016/j.apcata.2006.06.031.
[61] E. Kertalli, J.C. Schouten, T.A. Nijhuis, Effect of hydrogen and propylene on the hydrogen peroxide decomposition over Pt, PtO and Au catalysts, Appl. Catal. A 538 (2017) 131–139, https://doi.org/10.1016/j.apcata.2017.03.023.